Research
Frontiers in Medical Case Reports, ISSN: 2582-8142
DOI: https://dx.doi.org/10.47746/FMCR.2026.7303

Machine Learning Models Based on Clinical–Radiological and Radiomics Features for Preoperative Prediction of Locoregional Staging in Pediatric Wilms Tumor

Jian Tao[1] | Zi Xu[1] | Haiyan Ma[1] | Fang Wang[2] | Xianchun Zeng[1*] | Yunsong Peng[1*]

***Correspondence:** Xianchun Zeng and Yunsong Peng
Address: [1]Department of Radiology, Guizhou Provincial People's Hospital, Guiyang, China; [2]Department of Research and Development, Shanghai United Imaging Intelligence, Shanghai, China
E-mail ✉: zengxianchun04@foxmail.com; pys@mail.ustc.edu.cn
Received: 03 May 2026; **Accepted:** 15 May 2026

ABSTRACT

Purpose: To explore the value of machine learning models based on clinical–radiological and radiomics features to preoperatively predict locoregional staging in pediatric Wilms tumor (WT). Materials and Methods: We enrolled 95 cases of pediatric WT confirmed by postoperative pathology (training cohort: n = 66, test cohort: n = 29). Using the WT staging system of the Children's Oncology Group, patients were divided into two groups, stage I (n = 60) and stage II–III (n = 35). We used univariate and multivariate regression to analyze clinical and radiological features and identify clinical independent predictors. Radiomics features were extracted from preoperative portal venous-phase images of abdominal computed tomography scans. We screened for the optimal radiomics features using dimensionality reduction and selection. Logistic regression (LR), random forest (RF), and support vector machine (SVM) models, were developed based on the selected optimal radiomics features and clinical independent predictors. The predictive performance and clinical benefit of each model were assessed using the receiver operating characteristic curve, calibration curve, and decision curve analysis (DCA). The performance of each model was comprehensively evaluated using area under the curve (AUC), accuracy, and F1 score. Results: Tumor morphology was the only clinically independent predictor. In total, ten optimal radiomics features were selected. The predictive performance of the models was good, with RF having the best overall performance. In the test cohort, the AUCs for the RF, LR, and SVM models were 0.737, 0.727, and 0.712, respectively, the F1 scores were 0.615, 0.583, and 0.583, respectively, and consistent accuracy was 65.5% for all models. The calibration curves indicated good consistency between the actual and predicted results for each model. The DCA indicated that all three models provided clinical net benefits. Conclusion: Machine learning models based on radiomics features and tumor morphology can preoperatively predict locoregional staging of pediatric WT.

Keywords: *Wilms Tumor, Clinical Staging, Tomography, X-Ray Computed, Radiomics, Machine Learning*

DOI: https://dx.doi.org/10.47746/FMCR.2026.7303

Introduction

Wilms tumor (WT) is the most prevalent malignant kidney tumor in children, accounting for more than 90% of all primary renal tumors in young children (Jha *et al*., 2023). Over the last few decades, most children with WT had a good prognosis, with population-based 5-year overall survival rates exceeding 90% (Vujanić *et al*., 2022). However, approximately 20% of patients are at risk of relapse predominantly within 2 years of diagnosis. The overall survival rate after relapse is approximately 50% (Spreafico *et al*., 2021). The locoregional stage is a well-established risk factor for local relapse, independent of distant metastases (Morin *et al*., 2021). The mainstay of adjuvant therapy for WT is chemotherapy. Studies have shown that patients with stage I WT can undergo nephron-sparing surgery or nephrectomy alone without postoperative chemotherapy (Neagu *et al*., 2025; Salzillo *et al*., 2025). Children diagnosed with stage II–III WT usually undergo chemotherapy and/or abdominal radiotherapy together with nephrectomy (Salzillo *et al*., 2025). Initial tumor staging of WT can be performed using contrast-enhanced computed tomography (CT) or magnetic resonance imaging (MRI) (Pater *et al*., 2021). However, traditional radiology has limited accuracy in determining the local staging of WT (Bălănescu *et al*., 2021; Schenk *et al*., 2021). Currently, the primary basis for local staging of WT comprises invasive surgical and pathological assessment (Balis *et al*., 2021; Artunduaga *et al*., 2023). Therefore, the development of a noninvasive and reliable method for predicting the locoregional staging of pediatric WT may help guide preoperative clinical decision-making and prognostic evaluation.

Radiomics is a method of obtaining high-throughput quantitative features from conventional medical images. Analysis of these features may yield noninvasive biomarkers to support clinical decision-making (Zhang *et al*., 2020). Recently, radiomics based on quantitative parameters obtained from CT or MRI images have proved useful for determining the T stage in various tumor types (Liu *et al*., 2024; Yang *et al*., 2021; Demirjian *et al*., 2022; Fang *et al*., 2024). However, few studies have investigated the application of radiomics in pediatric malignant renal tumors (Shin *et al*., 2019; Deng *et al*., 2024; Ma *et al*., 2022). Furthermore, only one study to date has demonstrated that a CT-based radiomics model can accurately predict WT stage I and non-stage I disease in pediatric patients preoperatively (Ma *et al*., 2022). Given that distant hematogenous metastases and bilateral renal involvement (stage IV and V WT) can be accurately detected on diagnostic CT, this approach can be used to differentiate between stage I and stage II–III WT preoperatively. In addition, the radiomics model in that study (Ma *et al*., 2022) did not incorporate CT radiological features, which limited its predictive power. Clinical radiological information can be used to improve the predictive power of radiomics models, as has been reported in the literature (Zheng *et al*., 2022).

Previous studies have indicated that the use of machine learning algorithms is associated with the increased predictive performance of radiomics models (Zheng *et al*., 2022; Xiao *et al*., 2023). The success of radiomics applications in clinical care can be driven by highly accurate and reliable machine learning approaches. Identifying optimal machine learning methods for radiomics applications is crucial for developing stable and clinically relevant radiomics biomarkers (Avanzo *et al*., 2020). Therefore, it is essential to compare different machine learning models for radiomics-based clinical biomarkers.

To the best of our knowledge, no studies have investigated the potential of radiomics combined with machine learning for predicting the locoregional staging of pediatric WT. This study aimed to develop and validate various machine learning models that integrate clinical–radiological and radiomics features to predict the locoregional staging (stage I vs. stage II–III) of pediatric WT, which is challenging to identify using conventional imaging.

Materials and Methods

Patients

We conducted a retrospective analysis of consecutive hospitalized pediatric patients with WT at our institution from January 2014 to June 2024. Approval of this study (Protocol code [2025-054]) was obtained from the institutional review board of Guizhou Provincial People's Hospital, and informed consent was waived because of the retrospective nature of the study. Inclusion criteria included (1) having received an abdominal contrast-enhanced CT scan before surgery, biopsy, chemotherapy, or radiotherapy; (2) intraoperative lymph node sampling and biopsy; and (3) postoperative pathology confirming WT. Exclusion criteria included (1) the presence of distant metastasis, (2) bilateral WT, and (3) CT images affected by severe motion artifacts. A total of 95 pediatric WT patients were ultimately enrolled in this study. The details of the patient recruitment flow are presented in Fig. 1.

Locoregional Staging of WT

Patients diagnosed with WT were categorized into two groups according to the Children's Oncology Group staging criteria (Spreafico *et al*., 2021): the stage I group and the stage II–III group. Stage I involves a tumor that is confined to the kidney with an intact renal capsule, has not ruptured or been biopsied before surgical resection, and has not invaded the renal sinus. Stage II involves a tumor that extends beyond the kidney and/or involves the renal sinus but is completely resected. Stage III disease is characterized by preoperative tumor rupture, intraoperative spill, or retroperitoneal lymph node involvement confirmed on

pathological evaluation. Among the 95 patients recruited in this study, there were 60 cases of stage I disease, 20 cases of stage II disease, and 15 cases of stage III disease.

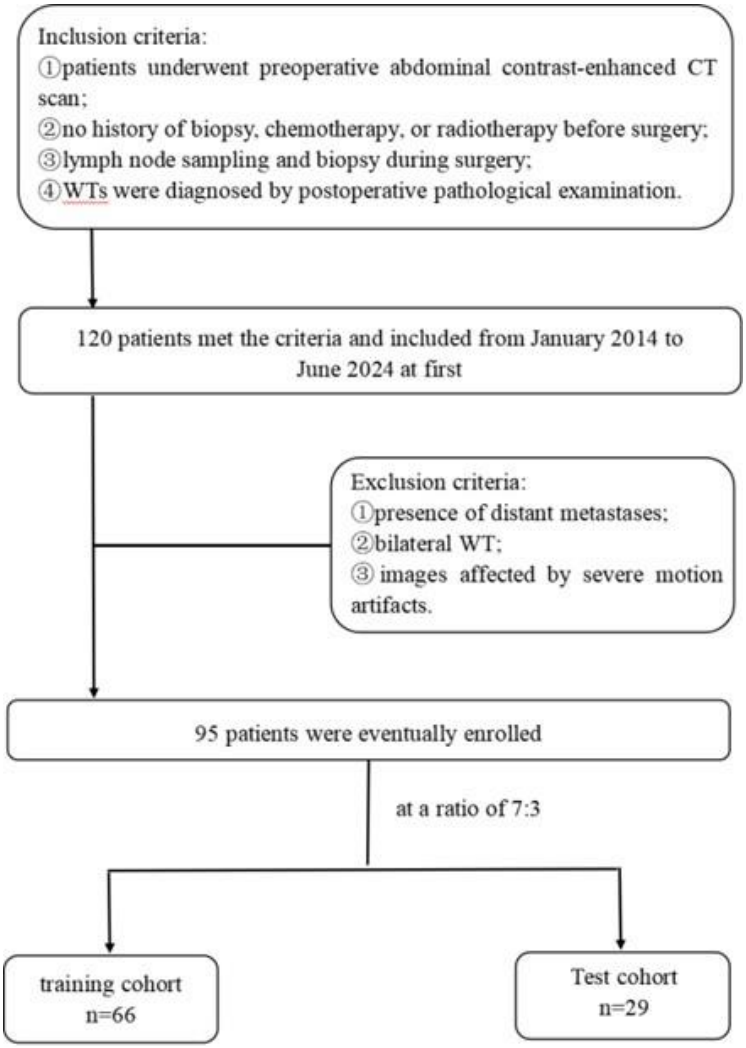

Figure 1: Flowchart for selecting the study population.

CT Image Acquisition

CT scans were conducted for all patients using one of the following systems: SOMATOM Definition, SOMATOM Definition AS 128, SOMATOM Perspective 128, and SOMATOM Force 256. The parameters for scanning were set as follows: tube voltage of 120 kV, tube current ranging from 200 to 400 mAs, field of view of 350 × 350–500 × 500 mm, and slice thickness of 5 mm. A contrast material bolus of 1.3–1.5 mL/kg body weight was administered intravenously at a rate of 1.5–2 mL/sec. After the enhancement of the descending aorta to 100 HU, arterial phase scanning began approximately 20–25 seconds later using a

bolus-tracking technique. Portal venous-phase images were obtained 60–75 seconds after contrast injection.

Clinical and Radiological Feature Analysis

1. Clinical feature collection: This included patient sex and age.

2. CT radiological feature evaluation: Two radiologists with more than 5 years of experience in abdominal diagnosis with unknown pathological results jointly analyzed the following CT radiological features of the tumor: maximum tumor diameter, tumor location (left or right kidney), tumor morphology (quasi-circular/elliptical vs. lobulated/irregular shaped), enlarged lymph nodes (presence or not; defined as the short diameter of the retroperitoneal lymph node ≥7 mm), contralateral tumor extension (presence or not; defined as a tumor extending beyond the midline of the vertebral body), displacement of great vessels (presence or not; considered when a left-sided tumor compressed the abdominal aorta or a right-sided tumor compressed the inferior cava vein), rich blood supply (presence or not; defined as prominent vessels within the tumor visible in the arterial phase), well-defined margin of the tumor (presence or not; evaluated as clear delineation of the edge of the tumor), retroperitoneal fluid (presence or not; considered fluid in the subcapsular, perirenal, or pararenal space), ascites (presence or not; considered present only if peritoneal fluid was present beyond the cul-de-sac), and ipsilateral pleural effusion (presence or not). In case of disagreement, consensus was reached by discussion.

3. Selection of clinical and radiological features: The clinical and radiological features were compared between groups using univariate logistic regression analysis. The statistically significant variables from the univariate analysis were then subjected to multivariate logistic regression analysis. Odds ratios as estimates of relative risk with 95% confidence intervals (CIs) were calculated for each independent predictor.

Radiomics Feature Extraction and Selection

1. Image selection and standardization: Cross-sectional portal venous-phase images of the abdominal CT, with the largest solid component of the tumor, were obtained for image feature extraction, and the slice thickness was 5 mm. Before feature extraction, CT image intensities were normalized between $\mu - 3\sigma$ and $\mu + 3\sigma$, where μ is the mean value of gray levels inside the region of interest (ROI) and σ is the standard deviation. Gray levels between $\mu - 3\sigma$ and $\mu + 3\sigma$ were then decimated to 64 gray levels.

DOI: https://dx.doi.org/10.47746/FMCR.2026.7303

2. *Feature extraction:* Using the MaZda software (version 4.6) to extract radiomics features, six types of features were generated: the histogram, the gray-level co-occurrence matrix, the gray-level run-length matrix, the absolute gradient, the auto-regressive model, and the Haar wavelet. The ROI was manually segmented along the tumor contour by two radiologists (Reader 1 and Reader 2, both with more than 5 years of experience) who were blinded to the pathological findings. Both Reader 1 and Reader 2 repeated the same procedure 2 months later to evaluate the intra-observer reproducibility. In addition, inter-observer reproducibility was evaluated between the two readers.

3. *Feature selection:* Before feature selection, each radiomics feature value was normalized using a Z-score. First, the intraclass correlation coefficients (ICCs) between the features extracted by the two radiologists were calculated; then, features with either intra-observer or inter-observer ICCs of less than 0.75 were excluded. Spearman's correlation analysis was used to screen features in the training cohort, and features with p values of less than 0.05 were retained. The minimum redundancy maximum relevance algorithm was then used to eliminate redundant and irrelevant features, and 20 highly predictive features were selected as the initial feature subset. Finally, the least absolute shrinkage and selection operator algorithm with 10-fold cross-validation was used to identify the optimal discriminative features. Features with coefficients reduced down to zero were removed, and the remaining nonzero features were selected.

Machine Learning Model Construction

In this study, we selected three mainstream machine learning algorithms, namely, logistic regression (LR), random forest (RF), and support vector machine (SVM), to construct prediction models based on the selected optimal radiomics features and clinical independent predictors. LR is a supervised learning algorithm used for solving binary classification problems. It is based on the principle of using logistic functions (also known as sigmoid functions) to model the probabilistic relationship between the dependent variable (output) and the independent variable (input). By building a probabilistic model, LR can predict the probability that a sample belongs to a particular category and find the optimal model parameters through an optimization algorithm (Zabor *et al*., 2022). RF is an ensemble learning method that constructs multiple decision trees through bootstrap sampling and random feature selection from the training set data, and finally integrates the predictions from all the decision trees to obtain the final prediction through a voting process (Borstelmann, 2020). SVM is a supervised learning algorithm mainly used for classification problems. Its basic principle is to find an optimal hyperplane in the feature space that maximizes the distance between different classes, thus improving classification accuracy (Borstelmann, 2020). An overview of the present study's workflow is presented in Fig. 2.

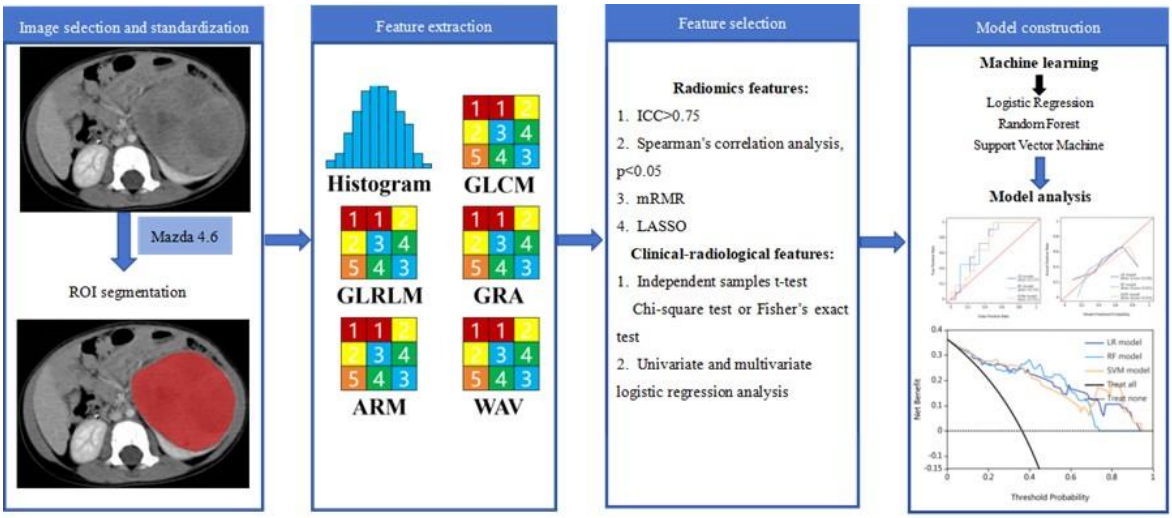

Figure 2: Workflow of this study.

Statistical Analysis

Statistical analysis was conducted using SPSS software (version 23, Chicago, IL, USA). For continuous variables, the Shapiro–Wilk test was performed first to verify their adherence to normal distribution. Independent-samples t test or nonparametric Mann–Whitney U test was then used to compare differences between groups. For categorical variables, the chi-square test or Fisher's exact test was used when appropriate. A two-tailed p value of less than 0.05 indicates that the difference is statistically significant.

The receiver operating characteristic curve, calibration curve, and decision curve analysis were used to evaluate the predictive performance and clinical benefit of each model. The performance of each model was comprehensively evaluated using three indicators: area under the curve (AUC), accuracy, and F1 score.

Results

1. Baseline Characteristics of Patients in The Training and Test Cohorts

The baseline patient characteristics of the training and test cohorts are presented in Table 1. There were no significant differences in the baseline patient characteristics between the training and test cohorts, indicating good consistency between the two data sets.

In the training cohort, the results of the univariate logistic regression analysis suggested that tumor morphology and well-defined margin of the tumor were predictors of locoregional staging in pediatric WT

(p = 0.011 and p = 0.034, respectively). After multivariate logistic regression analysis, tumor morphology was found to be an independent predictor for the locoregional staging of pediatric WT (odds ratio, 3.354; 95% CI, 1.122–10.030; p = 0.030) (Table 2).

Table 1: Comparison of the clinical and radiological features of patients in the training and test cohorts. (categorical variables are expressed in terms of totals and percentages)

Variables	Training (n=66)	Test (n=29)	χ2/t	P
Sex				
Male	38 (57.6)	19 (65.5)	0.529	0.467
Female	28 (42.4)	10 (34.5)		
Age (mean ± sd), years	2.27 ± 1.28	3.92 ± 3.06	-1.75	0.102
Maximum tumor diameter (mean ± sd), cm	9.87 ± 2.57	12.26 ± 3.73	-1.972	0.060
Tumor location				
left	44 (66.7)	17 (58.6)	0.568	0.451
right	22 (33.3)	12 (41.4)		
Tumor morphology				
Quasicircular or elliptical	41 (62.1)	21 (72.4)	0.941	0.332
Lobulated or irregular shaped	25 (37.9)	8 (27.6)		
Enlarged lymph node				
Present	23 (34.8)	9 (31.0)	0.131	0.717
Absent	43 (65.2)	20 (69.0)		
Contralateral tumor extension				
Present	25 (37.9)	11 (37.9)	0.000	0.996
Absent	41 (62.1)	18 (62.1)		
Displacement of great vessels				
Present	28 (42.4)	12 (41.3)	0.009	0.924
Absent	38 (57.6)	17 (58.7)		
Well-defined margin				
Present	28 (42.4)	14 (48.3)	0.280	0.597
Absent	38 (57.6)	15 (51.7)		
Rich blood supply				
Present	40 (60.6)	15 (51.7)	0.652	0.419
Absent	26 (39.4)	14 (48.3)		
Retroperitoneal fluid				
Present	30 (45.5)	12 (41.4)	0.136	0.713
Absent	36 (54.5)	17 (58.6)		
Ascites				
Present	29 (43.9)	11 (37.9)	0.298	0.585
Absent	37 (56.1)	18 (62.1)		
Ipsilateral pleural effusion				
Present	16 (24.2)	6 (20.7)	0.143	0.705
Absent	50 (75.8)	23 (79.3)		

Table 2: Univariate and multivariable logistic regression analyses for selecting clinical and radiological features.

Variable	Univariate analysis		Multivariate analysis	
	OR (95% CI)	p-value	OR (95% CI)	p-value
Sex	0.357 (0.127, 1.005)	0.051		
Age (years)	1.125 (0.874, 1.447)	0.360		
Maximum tumor diameter (cm)	1.087 (0.918, 1.288)	0.332		
Tumor location	1.846 (0.606, 5.626)	0.281		
Tumor morphology	3.945 (1.362, 11.431)	0.011*	3.354 (1.122, 10.030)	0.030*
Enlarged lymph node	0.628 (0.221, 1.780)	0.381		
Contralateral tumor extension	0.778 (0.278, 2.174)	0.632		
Displacement of great vessels	0.550 (0.194, 1.560)	0.261		
Well-defined margin	3.300 (1.093, 9.960)	0.034*	2.695 (0.853, 8.517)	0.091
Rich blood supply	0.367 (0.121, 1.107)	0.075		
Retroperitoneal fluid	0.750 (0.274, 2.053)	0.575		
Ascites	0.680 (0.248, 1.867)	0.454		
Ipsilateral pleural effusion	0.471 (0.150, 1.480)	0.197		

*Represents $p < 0.05$. OR odds ratio, CI confidence interval

2. Radiomics Feature Extraction and Selection

A total of 279 texture features were extracted for each patient using the MaZda software. Of the 279 features, 258 were demonstrated to have good inter-observer and intra-observer reproducibility, with ICCs > 0.75. Of the remaining features, 223 were retained with p values of less than 0.05 using Spearman's correlation analysis. Then, the minimum redundancy maximum relevance algorithm was used to eliminate redundant and irrelevant features, and 20 features were retained. Finally, 10 optimal radiomics features were selected using the least absolute shrinkage and selection operator algorithm, including five gray-level co-occurrence matrix features, three gray-level run-length matrix features, one auto-regressive model feature, and one Haar wavelet feature.

3. Prediction Performance of Three Machine Learning Models

Based on 10 optimal radiomics features and tumor morphology, the predictive performances of the three machine learning models were found to be relatively good, with RF having the best overall performance. In the test cohort, the RF model had the highest AUC (0.737), followed by LR (AUC=0.727) and SVM (AUC=0.712). All three models had a consistent accuracy (65.5%). Additionally, the RF model had the highest F1 score (0.615); the LR and SVM models both had F1 scores of 0.583 (Table 3 and Fig. 3). The calibration curve revealed that each model had good consistency between the actual and predicted results in the training and test cohorts, indicating good calibration performance (Fig. 4). The decision curve analysis indicated that all three machine learning models provided a certain clinical net benefit (Fig. 5).

In this study, radiomics feature selection, machine learning model construction, and performance evaluation were all performed on the uRP platform (Wu *et al*., 2023) developed by the Shanghai United

Imaging Intelligence Company. Detailed information regarding the parameters of the three machine learning models is shown in Table 4.

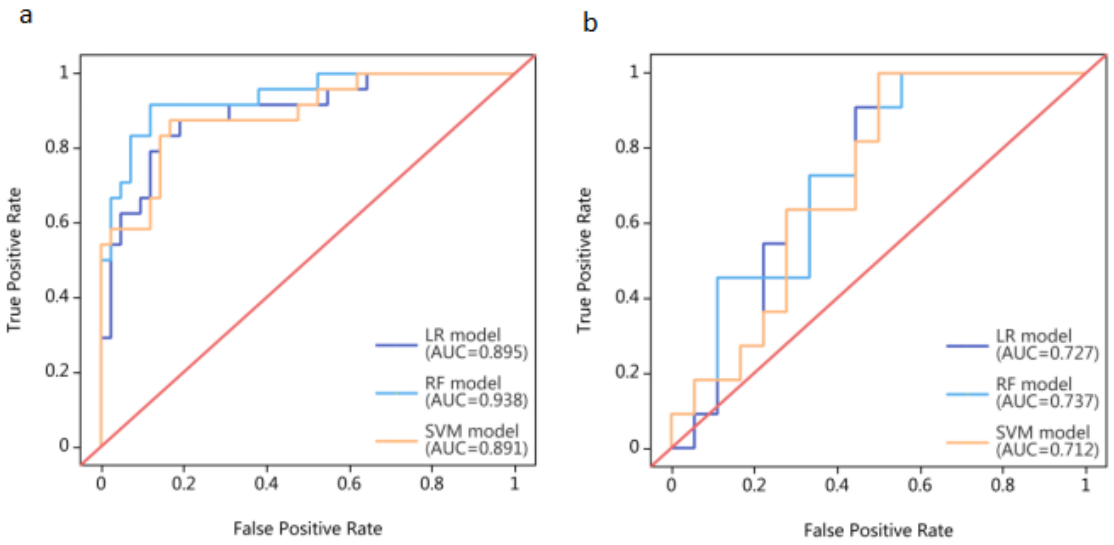

Figure 3: Receiver operating characteristic (ROC) curves of the LR model, RF model, and SVM model in the training (a) and test (b) cohorts, respectively. LR, logistic regression; RF, random forest; SVM, support vector machine.

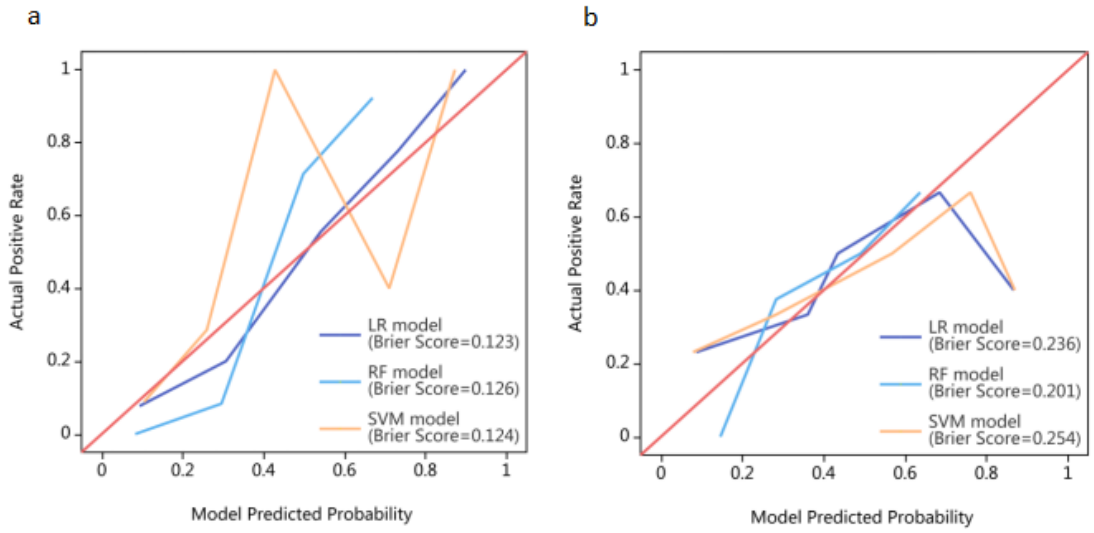

Figure 4: Calibration curves of three models for predicting locoregional staging of pediatric WT in the training (a) and test (b) cohorts, respectively.

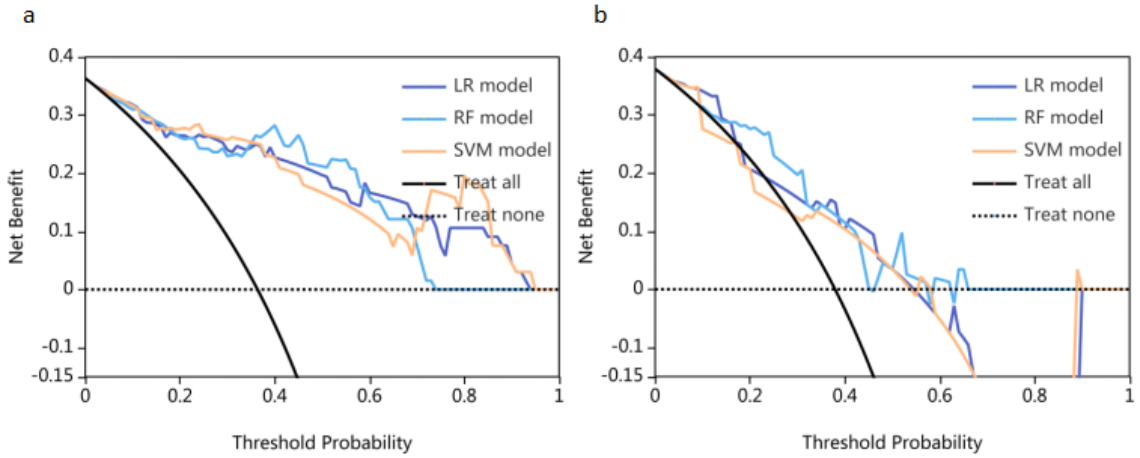

Figure 5: Decision curve analysis (DCA) for three models in predicting locoregional staging of pediatric WT in the training **(a)** and test **(b)** cohorts, respectively..

Table 3: Diagnostic performance of three machine learning models for predicting the locoregional staging of pediatric Wilms tumor in the training and test cohorts.

Model		AUC (95% CI)	accuracy	sensitivity	specificity	F1 score
LR	Training	0.895 (0.814-0.976)	83.3%	0.792	0.857	0.776
	Test	0.727 (0.541-0.913)	65.5%	0.636	0.667	0.583
RF	Training	0.938 (0.878-0.997)	89.4%	0.917	0.881	0.863
	Test	0.737 (0.554-0.920)	65.5%	0.727	0.611	0.615
SVM	Training	0.891 (0.808-0.974)	83.3%	0.792	0.857	0.776
	Test	0.712 (0.523-0.902)	65.5%	0.636	0.667	0.583

Table 4: Detailed information on the parameters of the three machine learning models.

Classifier	Model Parameters						
LR	C	Penalty	Tol	Threshold	Youden Threshold		
	1.0	l2	0.0001	0.50	0.14		
RF	Criterion	Max Depth	Min Samples Leaf	Min Samples Split	N Estimators	Threshold	Youden Threshold
	Gini	2	1	2	100	0.40	0.24
SVM	C	Gamma	Kernel	Threshold	Youden Threshold		
	1.0	0.01	Rbf	0.50	0.10		

Discussion

The present study employed three machine learning methods to construct models for predicting the locoregional staging of pediatric WT based on the radiomics features extracted from portal venous-phase images of abdominal CT and tumor morphology. The results showed that the three machine learning models achieved good predictive performance in both the training and test cohorts, which provided a noninvasive and effective method for preoperative clinical decision-making and prognostic assessment.

Radiomics has the potential to aid in the development of predictive diagnostics for personalized medicine. The diagnostic efficacy of radiomics models is related to the choice of machine learning algorithm (Zheng *et al*., 2022; Xiao *et al*., 2023); however, most studies that reported the use of radiomics in other tumor applications randomly applied a machine learning classifier, and comparative studies evaluating the strengths and weaknesses of different machine learning algorithms and their diagnostic efficacy are scarce. Liu, *et al*. (2024) constructed seven machine learning models based on radiomics features extracted from CT images for the purpose of distinguishing between T2 and T3 staging of laryngeal and hypopharyngeal squamous cell carcinoma. They reported that LR achieved the optimal diagnostic performance across the training, test, and validation sets. In a separate study, Artzi, *et al*. (2019) used four machine learning algorithms to identify glioblastoma and brain metastases of different origins based on enhanced T1WI and found that the SVM model achieved the best diagnostic efficacy. In a similar study, Fang, *et al*. (2024) used four machine learning models to predict postoperative recurrence in patients with chronic subdural hematoma. The authors reported that the SVM model exhibited superior prediction accuracy. Zhao, *et al*. (2023) constructed three radiomics models to differentiate between primary central nervous system lymphoma and brain metastases, with the RF model performing the best.

As previously mentioned, LR, RF, and SVM are common and well-established machine learning algorithms that are used in radiomics research. LR is a linear classifier, with the advantages of interpretability and high computational efficiency for binary classification problems. It is suitable for scenarios where there is a linear relationship between features and target variables (Schober and Vetter, 2021). RF can capture complex non-linear relationships without the need to normalize the data. It improves the generalization and overfitting resistance of the model through integrated learning. RF performs well when the relationship between the features of the data and the target variable is complex and non-linear, or when there are a large number of features (Jiang *et al*., 2020). SVM can control for non-linear relationships and is suitable for high-dimensional data by extending to high-dimensional spaces through kernel functions. It is suitable for small- and medium-sized datasets and performs well when the data is non-linearly differentiable (Valkenborg *et al*., 2023). Thus, different machine learning models have different characteristics and different scopes of applicability. In this study, we selected these three mainstream machine learning algorithms to construct predictive models, and the results indicated that the RF model exhibited slightly superior predictive performance compared with the LR and SVM models. The predictive performance of an RF is often comparable with that of the best available machine learning models due to its ability to handle missing data and integrate various feature types (Becker *et al*., 2023). When used in conjunction with most feature selection methods, the RF model often achieves the highest predictive performance (Avanzo *et al*., 2020).

This study has several limitations. First, it is a single-center retrospective study with a limited sample size, potentially introducing selection bias. To enhance the reliability of the findings, further validation is required using a larger patient cohort from multiple centers. Second, ROIs were manually outlined on cross-sectional images of the largest solid component of the tumor, potentially missing the spatial heterogeneity of the entire tumor. Finally, the CT images were obtained from a variety of CT scanners, potentially affecting the consistency of the results, although standardized pre-processing procedures were implemented to minimize these variations.

Conclusion

In conclusion, machine learning models based on radiomics features and tumor morphology demonstrated good diagnostic performance in predicting the locoregional staging of pediatric WT, which may provide a noninvasive and robust approach to optimize preoperative clinical decision-making.

Acknowledgments: We thank LetPub (www.letpub.com.cn) for linguistic assistance and pre-submission expert review.

Funding: This work was supported by the Guizhou Provincial People's Hospital Talent Fund (Peng Yunsong) under Grant Hospital Talent Project [2022]-5.

Competing Interest: None

Ethical Statement: This retrospective, single-center study was approved by the Institutional Review Board.

Data Availability: The data that support the findings of this study will be made available on reasonable request.

References

Artunduaga M, Eklund M, van der Beek JN, Hammer M, Littooij AS, Sandberg JK, Schenk JP, Servaes S, Singh S, Smith EA, Srinavasan A, Khanna G. Imaging of pediatric renal tumors: A COG Diagnostic Imaging Committee/SPR Oncology Committee White Paper focused on Wilms tumor and nephrogenic rests. *Pediatr Blood Cancer* 2023; 70: e30004.

Artzi M, Bressler I, Ben Bashat D. Differentiation between glioblastoma, brain metastasis and subtypes using radiomics analysis. *J Magn Reson Imaging* 2019; 50: 519-528.

Avanzo M, Wei L, Stancanello J, Vallières M, Rao A, Morin O, Mattonen SA, El Naqa I. Machine and deep learning methods for radiomics. *Med Phys* 2020; 47: e185-e202.

Bălănescu RN, Bălănescu L, Strîmbu TS, Cardoneanu AM, Moga AA. Prediction of histopathological local staging by radiological findings and differential diagnosis overview in children with nephroblastoma. *Rom J Morphol Embryol* 2021; 62: 939-949.

Balis F, Green DM, Anderson C, Cook S, Dhillon J, Gow K, Hiniker S, Jasty-Rao R, Lin C, Lovvorn H, MacEwan I, Martinez-Agosto J, Mullen E, Murphy ES, Ranalli M, Rhee D, Rokitka D, Tracy EL, Vern-Gross T, Walsh MF, Walz A, Wickiser J, Zapala M, Berardi RA, Hughes M. Wilms Tumor (Nephroblastoma), Version 2.2021, NCCN Clinical Practice Guidelines in Oncology. *J Natl Compr Canc Netw* 2021; 19: 945-977.

Becker T, Rousseau AJ, Geubbelmans M, Burzykowski T, Valkenborg D. Decision trees and random forests. *Am J Orthod Dentofacial Orthop* 2023; 164: 894-897.

Borstelmann SM. Machine Learning Principles for Radiology Investigators. *Acad Radiol* 2020; 27: 13-25.

Demirjian NL, Varghese BA, Cen SY, Hwang DH, Aron M, Siddiqui I, Fields BKK, Lei X, Yap FY, Rivas M, Reddy SS, Zahoor H, Liu DH, Desai M, Rhie SK, Gill IS, Duddalwar V. CT-based radiomics stratification of tumor grade and TNM stage of clear cell renal cell carcinoma. *Eur Radiol* 2022; 32: 2552-2563.

Deng Y, Wang H, He L. CT radiomics to differentiate between Wilms tumor and clear cell sarcoma of the kidney in children. *BMC Med Imaging* 2024; 24: 13.

Fang C, Ji X, Pan Y, Xie G, Zhang H, Li S, Wan J. Combining Clinical-Radiomics Features With Machine Learning Methods for Building Models to Predict Postoperative Recurrence in Patients With Chronic Subdural Hematoma: Retrospective Cohort Study. *J Med Internet Res* 2024; 26: e54944.

Fang R, Lin N, Weng S, Liu K, Chen X, Cao D. Multiparametric MRI radiomics improves preoperative diagnostic performance for local staging in patients with endometrial cancer. *Abdom Radiol* (NY) 2024; 49: 875-887.

Jha SK, Brown C, Kang L, Diaz ES, Gwal K, Alvarez E, Brown EG, Stein-Wexler R. Update on the Role of Imaging in Staging of Common Pediatric Abdominal Tumors. *Curr Probl Cancer* 2023; 47: 100969.

Jiang T, Gradus JL, Rosellini AJ. Supervised Machine Learning: A Brief Primer. *Behav Ther* 2020; 51: 675-687.

Liu Q, Liu S, Mao Y, Kang X, Yu M, Chen G. Machine learning model to preoperatively predict T2/T3 staging of laryngeal and hypopharyngeal cancer based on the CT radiomic signature. *Eur Radiol* 2024; 34: 5349-5359.

Ma XH, Shu L, Jia X, Zhou HC, Liu TT, Liang JW, Ding YS, He M, Shu Q. Machine Learning-Based CT Radiomics Method for Identifying the Stage of Wilms Tumor in Children. *Front Pediatr* 2022; 10: 873035.

Morin CE, Artunduaga M, Schooler GR, Brennan RC, Khanna G. Imaging for Staging of Pediatric Abdominal Tumors: An Update, From the AJR Special Series on Cancer Staging. *AJR Am J Roentgenol* 2021; 217: 786-799.

Neagu MC, David VL, Iacob ER, Chiriac SD, Muntean FL, Boia ES. Wilms' Tumor: A Review of Clinical Characteristics, Treatment Advances, and Research Opportunities. Medicina (Kaunas). 2025; 61: 491.

Pater L, Melchior P, Rübe C, Cooper BT, McAleer MF, Kalapurakal JA, Paulino AC. Wilms tumor. *Pediatr Blood Cancer* 2021; 68: e28257.

Salzillo C, Cazzato G, Serio G, Marzullo A. Paediatric Renal Tumors: A State-of-the-Art Review. *Curr Oncol Rep* 2025; 27: 211-224.

Schenk JP, Hötker A, Furtwängler R, Fuchs J, Warmann SW, Graf N. Bildgebung renaler Tumoren im Kindesalter [Imaging of renal tumors in children]. Radiologe 2021; 61: 619-628.

Schober P, Vetter TR. Logistic Regression in Medical Research. *Anesth Analg* 2021; 132: 365-366.

Shin HJ, Kwak JY, Lee E, Lee MJ, Yoon H, Han K, Kim MJ. Texture Analysis to Differentiate Malignant Renal Tumors in Children Using Gray-Scale Ultrasonography Images. *Ultrasound Med Biol* 2019; 45: 2205-2212.

Spreafico F, Fernandez CV, Brok J, Nakata K, Vujanic G, Geller JI, Gessler M, Maschietto M, Behjati S, Polanco A, Paintsil V, Luna-Fineman S, Pritchard-Jones K. Wilms tumour. *Nat Rev Dis Primers* 2021; 7: 75.

Valkenborg D, Rousseau AJ, Geubbelmans M, Burzykowski T. Support vector machines. *Am J Orthod Dentofacial Orthop* 2023; 164: 754-757.

Vujanić GM, Parsons LN, D'Hooghe E, Treece AL, Collini P, Perlman EJ. Pathology of Wilms' tumour in International Society of Paediatric Oncology (SIOP) and Children's oncology group (COG) renal tumour studies: Similarities and differences. *Histopathology* 2022; 80: 1026-1037.

Wu J, Xia Y, Wang X, Wei Y, Liu A, Innanje A, Zheng M, Chen L, Shi J, Wang L, Zhan Y, Zhou XS, Xue Z, Shi F, Shen D. uRP: An integrated research platform for one-stop analysis of medical images. *Front Radiol* 2023; 3: 1153784.

Xiao DX, Zhong JP, Peng JD, Fan CG, Wang XC, Wen XL, Liao WW, Wang J, Yin XF. Machine learning for differentiation of lipid-poor adrenal adenoma and subclinical pheochromocytoma based on multiphase CT imaging radiomics. *BMC Med Imaging* 2023; 23: 159.

Yang M, Hu P, Li M, Ding R, Wang Y, Pan S, Kang M, Kong W, Du D, Wang F. Computed Tomography-Based Radiomics in Predicting T Stage and Length of Esophageal Squamous Cell Carcinoma. *Front Oncol* 2021; 11: 722961.

Zabor EC, Reddy CA, Tendulkar RD, Patil S. Logistic Regression in Clinical Studies. *Int J Radiat Oncol Biol Phys* 2022; 112: 271-277.

Zhang Q, Peng Y, Liu W, Bai J, Zheng J, Yang X, Zhou L. Radiomics Based on Multimodal MRI for the Differential Diagnosis of Benign and Malignant Breast Lesions. *J Magn Reson Imaging* 2020; 52: 596-607.

Zhao LM, Hu R, Xie FF, Clay Kargilis D, Imami M, Yang S, Guo JQ, Jiao X, Chen RT, Wei-Hua L, Li L. Radiomic-Based MRI for Classification of Solitary Brain Metastases Subtypes From Primary Lymphoma of the Central Nervous System. *J Magn Reson Imaging* 2023; 57: 227-235.

Zheng Y, Zhou D, Liu H, Wen M. CT-based radiomics analysis of different machine learning models for differentiating benign and malignant parotid tumors. *Eur Radiol* 2022; 32: 6953-6964.